DRI #2504

AFOSR 69-2052TR

REPORT

Final Report

Grant AFOSR-1079-66

May 1969

PYROLYSIS AND COMBUSTION OF LITHIUM ALUMINUM HYDRIDE

UNIVERSITY OF DENVER
DENVER RESEARCH INSTITUTE

42

PYROLYSIS AND COMBUSTION OF LITHIUM ALUMINUM HYDRIDE

William H. McLain
Franklin I. Honea

Final Report - Grant AFOSR-1079-66

Department of Environmental and Mechanical Sciences
Denver Research Institute
University of Denver

May 1969

Directorate of Engineering Sciences - Combustion Dynamics
Air Force Office of Scientific Research (OAR)
Arlington, Virginia

TABLE OF CONTENTS

LIST OF FIGURES

ABSTRACT

The slow pyrolysis of lithium aluminum hydride proceeds by a successive dehydrogenation of the fuel in three stages over a temperature range between 210° and 460°C. The combustion of lithium aluminum hydride follows a simular multistage process in which the pyrolytic dehydrogenation is followed by an afterburning of the metal substrate. Experimental studies were performed to determine the delay times between successive stages for solid mixtures of lithium aluminum hydride with selected oxidizers. Time resolved spectrographic techniques were used to determine the duration of these stages. Studies were performed using Li_2O_2 and NH_4NO_3 oxidizers over a particle size range between 75-300 microns and O/F mixture ratios of between 0.5 and 3.0. Ignition delay times for the initial reaction were found to vary between 5 and 40 milliseconds for the first stage and 10 to 120 milliseconds for the second stages. An analytical model was developed to describe the observed multistage combustion process. The model and resulting PARTIG computer program utilize the nodal approach with stepwise solution of the equations for heat and mass transfer. The analytically predicted ignition delay times for a 50μ particle agreed favorably with the experimentally obtained times.

I. INTRODUCTION

Advanced rocket propellant combinations include the use of light metal hydride fuels. The physical and chemical mechanisms important to the combustion of metal hydrides differ substantially from those associated with the combustion of nacent metals. For metal hydrides the combustion proceeds through an initial pyrolysis reaction which is then followed by the combustion of the metal substrate. The result is the existence of multistage reaction sequence in which the first stage has a relatively cool flame temperature which is then followed by a high temperature secondary combustion stage. Because of the time lag between these two stages, the combustion efficiency of metal hydride particles in a rocket engine is lowered relative to efficiencies for similar metal particles especially for short engine residence times. The extent to which these reactions are delayed is therefore of fundamental interest to propulsion engineering.

II. EXPERIMENTAL APPROACH

Lithium aluminum hydride - $LiAlH_4$ was chosen as a typical light metal hydride for the study of ignition and combustion processes. This fuel was chosen since it is of current interest for some propellant systems and secondly because its thermal degradation and physical properties are relatively well characterized. Thermal degradation of this compound proceeds through at least three separate steps.[1,2] Differential thermal analysis studies shown in Figure 1 schematically show the proposed reaction sequence for this degradation. These are correlated with experimental differential scanning calorimeter data presented in Figure 2. These experimental results clearly show the stepwise staging of the decomposition reactions which occur in the slow pyrolysis of this metal hydride.

To study the combustion process under fast reaction conditions, a series of experimental spectroscopic studies were performed to determine the time delay between the ignition of the first stage and the subsequent reaction sequence for fuel oxidizer mixtures of $LiAlH_4$ - Li_2O_2 and $LiAlH_4$-NH_4NO_3. Primary experimental variables were the particle size and O/F mixture ratios. The experimental procedure consisted of mixing the fuel and oxidizer as a powder in the appropriate mixture ratio. Ignition of the "solid propellant" was then accomplished by either spark or laser initiation. The reaction sequence was followed using a fast streak spectrograph. This spectrographic method allows a detailed

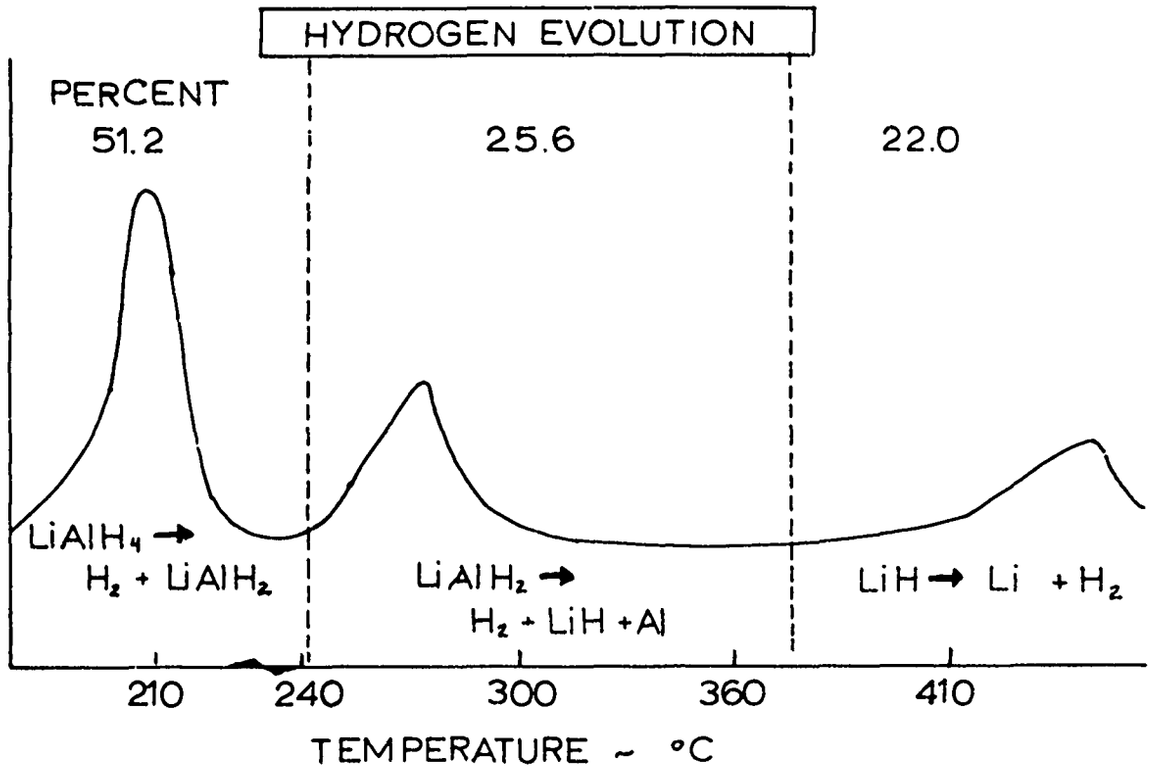

Figure 1. Reaction Sequence and Evolution of Hydrogen for $LiAlH_4$

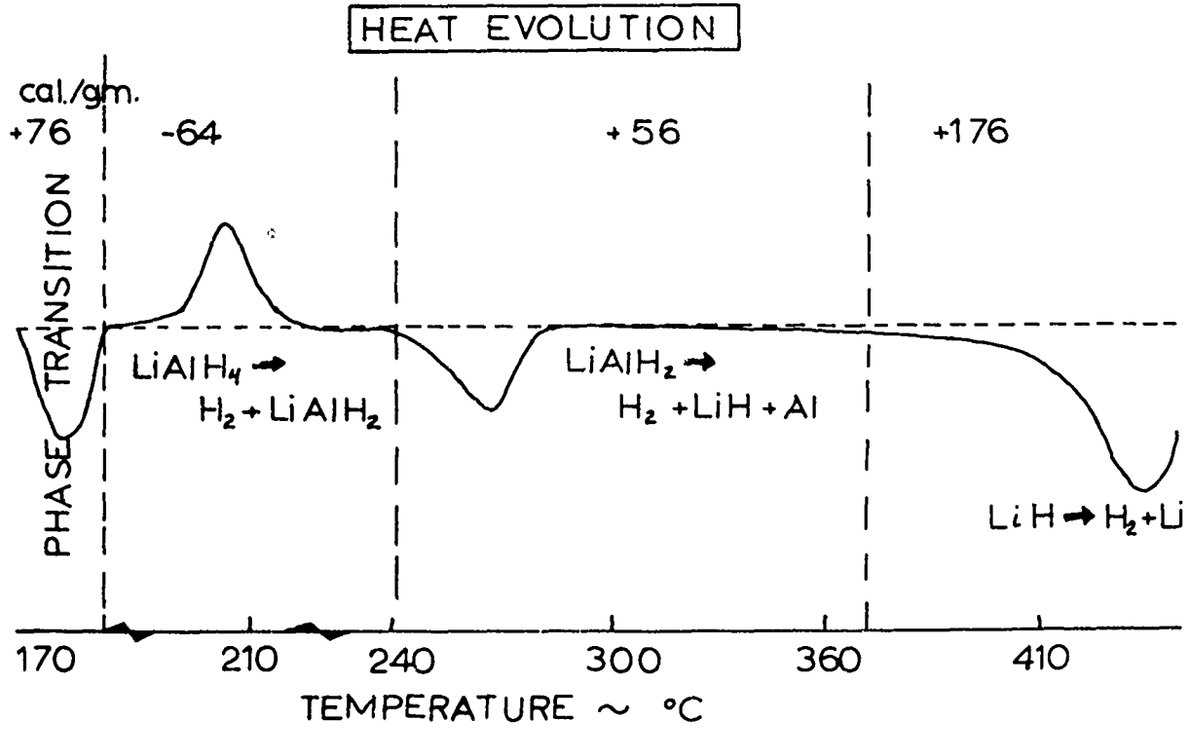

Figure 2. Differential Scanning Calorimetric Analysis for $LiAlH_4$

analysis of the buildup and staging of the reactions important to the ignition, pyrolysis and subsequent combustion of these powders.

A typical series of spectrographic records for the combustion of a mixture of $LiAlH_4$ - Li_2O_2 is given in Figure 3. On this record time "zero" is on the left hand side and reaction proceeds to the right. The gross features of this record include a single Li atomic emission line followed by a wider spectral response which corresponds to the first stage reaction. In the upper region a careful analysis indicates the probable existence of self-absorption bands in the region of the water bands. The second stage is then initiated as shown by the large increase in the blackbody emission. These wider bands include a marked blackbody continuum together with a reasonably well-defined self-absorption band at about 4800 Å, which corresponds to strong aluminum oxide bands. The series of records clearly show the effect of particle size variation on the onset of these processes. The particle size was varied to provide a semimonodisperse system having a particle diameter less than 300, 150 and 75 microns, respectively. As the particle size is reduced, the time required for the pyrolysis reaction is reduced from time zero as is the time delay between consecutive stages.

A systematic study of the effect of particle size vs time delay for these reactions was performed. Results of this study are given in Figures 4, 5, and 6. Figure 4 shows the variation of ignition delay time as a function of an area to mass ratio normalized to a 75μ particle size. Both steps of the reaction are shown together with the time delay between the stages. As can be observed, there is a very pronounced dependence of the ignition and staging delay time on the available surface area. Also there are major changes in the shape of curvature for small particles which is dependent on the oxidizer used. This latter effect shows the strong dependence of initiation on oxidative environment although insufficient data were available to investigate the pyrolysis of the oxidizer. Figures 5 and 6 show the effective time delay to ignition for the Stage I and Stage II reactions, respectively. These are plotted as a function of O/F mixture ratios for the $LiAlH_4$ - Li_2O_2 fuel oxidizer combination. Again the effect of particle size is pronounced.

Li_2O_2 (48) - $LiAlH_4$ (48)
O/F = 3

Li_2O_2 (48) - $LiAlH_4$ (100)
O/F = 3

Li_2O_2 (100) - $LiAlH_4$ (48)
O/F = 3

Li_2O_2 (100) - $LiAlH_4$ (100)
O/F = 3

Li_2O_2 (200) - $LiAlH_4$ (48)
O/F = 3

Li_2O_2 (200) - $LiAlH_4$ (100)
O/F = 3

TIME ⟶

Figure 3. Spectrographic Records $LiAlH_4$-Li_2O_2

Li_2O_2 (48) - $LiAlH_4$ (200)
O/F = 3

Li_2O_2 (100) - $LiAlH_4$ (200)
O/F = 3

Li_2O_2 (200) - $LiAlH_4$ (200)
O/F = 3

TIME ⟶

Figure 3 (Cont)

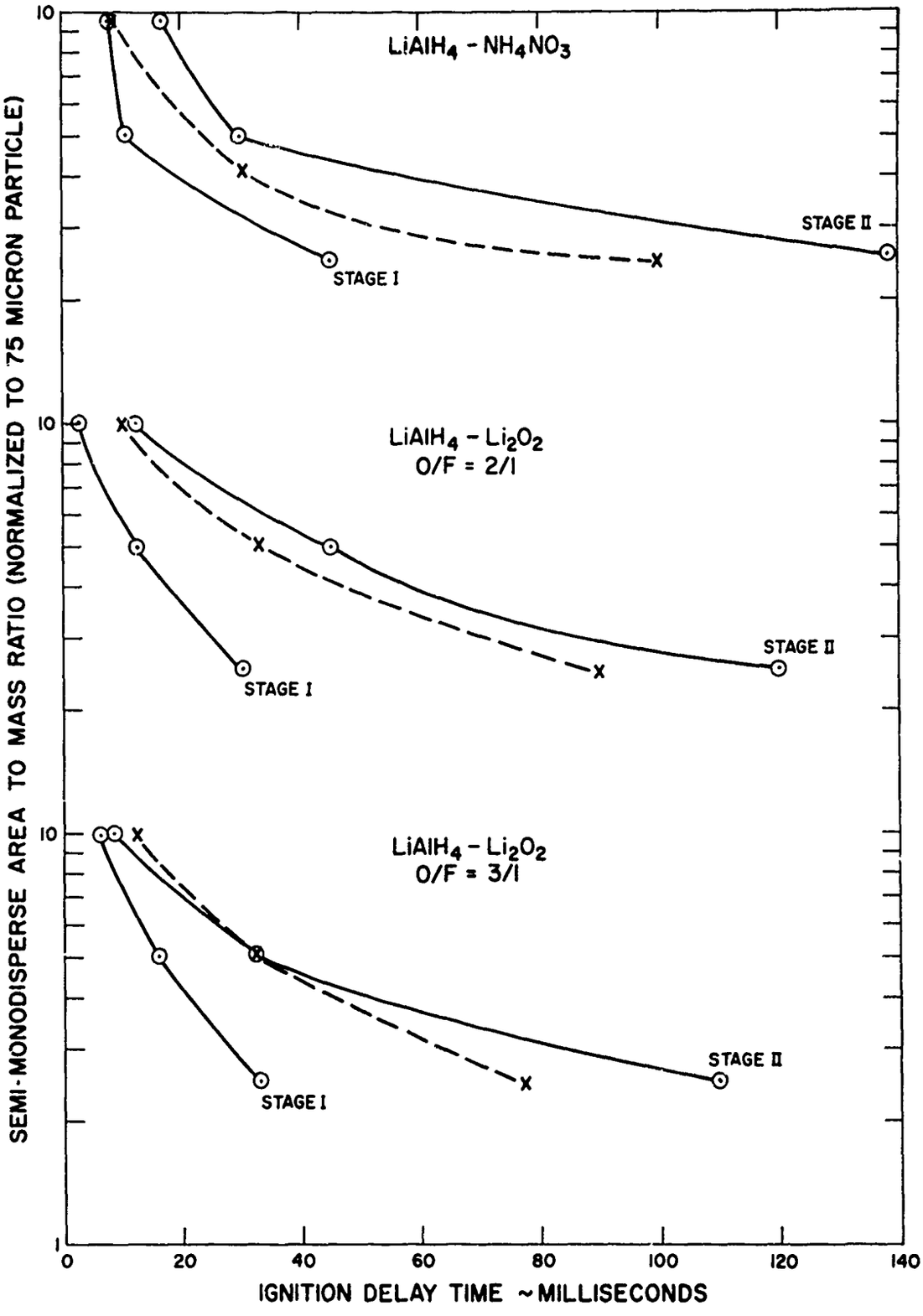

Figure 4. Typical Ignition Delay Times Normalized to 75μ Particle

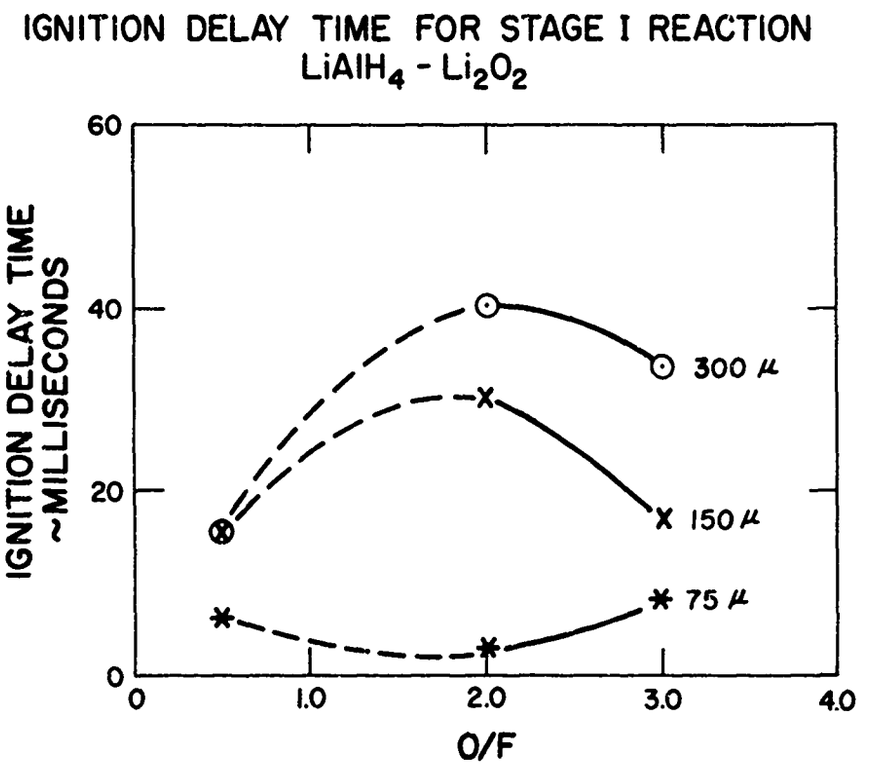

Figure 5. Time Delay to Ignition - Stage I Reaction

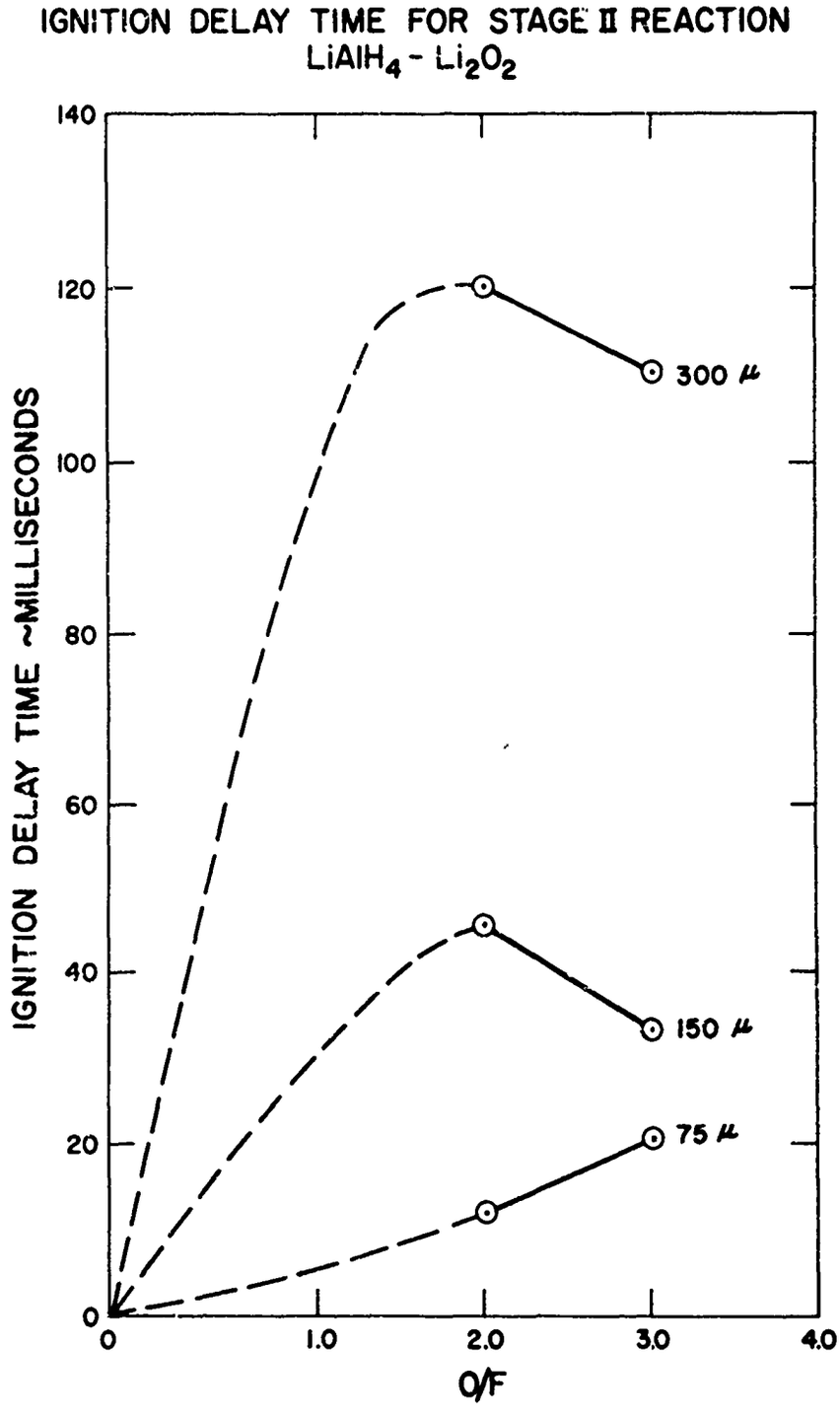

Figure 6. Time Delay to Ignition - Stage II Reaction

III. THEORETICAL APPROACH

A. Analytical Model

The experimental results for the ignition of lithium aluminum hydride indicate the presence of two stages of ignition. These two stages plus the porosity of the material and the resulting considerations of coupled mass and heat transfer within the material must be included in the model for ignition. Because of these added considerations, theoretical models describing light metal hydride ignition must be much more complex than the current models for the ignition of molten metallic particles.

Based on the experimental results, a model for the ignition has been formulated and is presented in Figure 7. The main steps during the transient period prior to final ignition include the following:

Step 1: Transient Heating - The particle is heated up from ambient conditions due to radiated and convective heat transfer.

Step 2: Stage I Ignition - The hydrogen is evolved and diffuses outward from the particle to the surface where ignition and combustion occurs.

Step 3: Lag Time - After the completion of hydrogen pyrolysis, a is provided to allow time for the oxygen to diffuse back to the surface.

Step 4: Oxidation - As the oxygen diffuses to the surface, the oxygen reacts with the exposed aluminum oxide.

Step 5: Vaporization - The continued heat transfer to the interior of the particle from the environment, and the hydrogen flame plus the heat generated from the hydrogen evolution and aluminum oxide formation result in eventual melting and vaporization of the core.

Step 6: Stage II Ignition - The vaporized metal diffuses outward from the particle and ignites when the proper thermal balance and concentrations of aluminum and oxygen are attained.

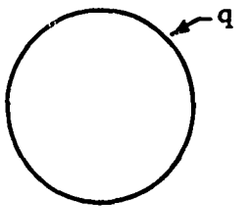

Step 1. Transient Heating

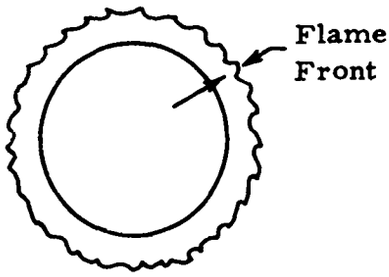

Step 2. Stage I Ignition

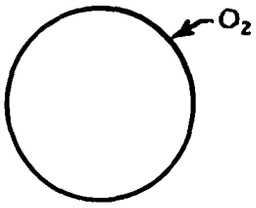

Step 3. Lag Time

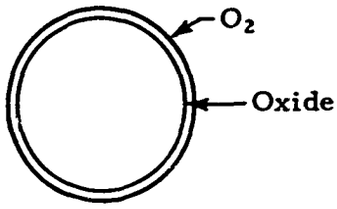

Step 4. Oxidation

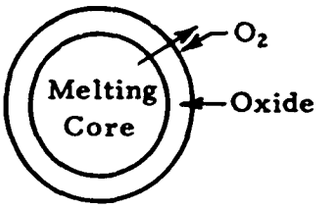

Step 5. Vaporization

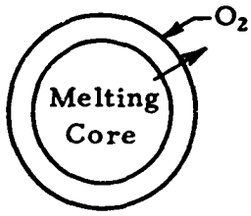

Step 6. Stage II Ignition

Figure 7. Hypothetical Model for Ignition of Light Metal Hydride Type Particles

The hypothetical model has been used as a basis for a digital computer program to predict the Stage I and Stage II ignition times and the variation of the hydrogen flame radius with time during hydrogen pyrolysis. The program utilizes the nodal approach with stepwise solution of differential equations. Reactions external to and within the spherical particle are assumed to be symmetrical so that the nodes are taken as concentric "onion skins" within the particle. Heat and mass balances are taken across each node. Whenever reactions occur the changes in mass and energy are added to the appropriate node within the sphere. The hydrogen pyrolysis and resulting flame zone external to the particle is treated by an appropriate energy balance including the enthalpies of the reaction and the reaching and product gases. The variation of the radius of the flame front is predicted by assuming a stable flame front with a linear variation in flame radius as a function of the total enthalpy difference available for the reaction. According to Brzustowski,[3] this assumption of linear variation is valid under certain conditions for stable flame zones.

A typical heat transfer balance across a node within the particle is illustrated in Figure 8. In this figure, the conductive heat transfer, the stored energy and chemical kinetic energy terms are all included. The energy balance becomes

$$(m C_p)_2 \left(\frac{dT}{dt}\right)_2 = k A_1 \left(\frac{dT}{dx}\right)_{1-2} - k A_2 \left(\frac{dT}{dx}\right)_{2-3} + q \qquad (1)$$

which can be modified by making the assumption that the derivatives can be approximated by the ratio of small increments of change

$$\left(\frac{dT}{dx}\right)_{1-2} \leftarrow \frac{T_1 - T_2}{\Delta x_{1-2}} \simeq \frac{T_1 - T_2}{R \Delta \zeta} . \qquad (2)$$

This assumption allows the substitution of increments into (1) to obtain

$$(m C_p)_2 \frac{(T_2' - T_2)}{\Delta t} = \frac{k}{R \Delta \zeta} [A_1(T_1 - T_2) - A_2(T_2 - T_3)] + q. \qquad (3)$$

This equation (3) can then be rearranged in the form

$$T_2' = T_2 + \frac{\Delta t}{(m C_p)_2} \left(\frac{k}{R \Delta \zeta}\right) [A_1(T_1 - T_2) - A_2(T_2 - T_3)] + \frac{\Delta t}{(m C_p)_2} (q) \qquad (4)$$

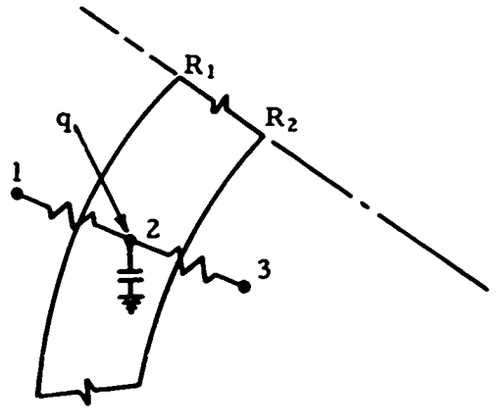

$$m_2 = \frac{4}{3}\pi (R_1^3 - R_2^3)\,\rho$$

$$A_1 = 4\pi R_1^2$$

$$\Delta x = R\,\Delta\,\zeta$$

Input: $-k A_1 \left(\frac{dT}{dx}\right)_{1-2}$

Output: $k A_2 \left(\frac{dT}{dx}\right)_{2-3}$

Stored: $(m C_p)_2 \left(\frac{dT}{dt}\right)_2$

Reaction Kinetics: q

Total: $(m C_p)_2 \left(\frac{dT}{dt}\right)_2 = k A_1 \left(\frac{dT}{dx}\right)_{1-2} - k A_2 \left(\frac{dT}{dx}\right)_{2-3} + q$

Figure 8. Typical Heat Balance Across A Node

which can readily be set up in FORTRAN IV or ALGOL language and solved.

An excellent discussion of shell balances and the terms for heat and mass transfer within spheres is included in the text by Bird, Stewart and Lightfoot.[4] The mass diffusion balance using node concentration levels and the effective diffusivity form is completely analogous with the heat transfer balance. The final form for stepwise differential solution is similar to (4)

$$C_2' = C_2 + \left(\frac{\Delta t}{\Delta V_2}\right)\left(\frac{D_e}{R\,\Delta\zeta}\right)[A_1(C_1 - C_2) - A_2(C_2 - C_3)] + \left(\frac{\Delta t}{\tau_2}\right) k_1 C_2^n \tag{5}$$

where $k_1 C^n$ is the term for change in concentration due to chemical reactions.

For the heat transfer at the surface of the particle, a quasi-steady-state balance is made between the heat input and the heat conducted into the sphere. The heat input includes radiation and convection from the environment and radiation from the flame zone when hydrogen pyrolysis is occurring.

For the mass transfer at the surface, the particle is assumed to be relatively at rest with respect to the environment so that forced mass transfer is not considered. Although the mass diffusion to and back from the flame zone is recognized as a major factor in flame dynamics and ignition delay by many sources including Kuehl and Zwillenberg,[5] the external diffusion for this program is considered simply as the diffusion of the reacting gas outward from the last node to the surface. Similarly, for diffusion of oxygen inward from the surface, the oxygen concentration in a normal, one atmosphere environment was considered as the driving potential. These approximations should not significantly affect the total ignition times. However, the time to ignition for Stage I may be predicted slightly prematurely since no time delay for diffusion of the hydrogen into the surrounding gaseous environment is included.

The computer program has been written in ALGOL language since an extended Burroughs B5500 is available at the Denver Research Institute. This program has been named as the PARTIG Program for

particle ignition. An iterative technique was used for solving the stepwise differential equations (4) and (5) for heat and mass transfer at each node. Again, the heat and mass transfer reiterative techniques are analogous so that the computer flow diagrams for both are similar. The reiterative flow diagram for heat transfer is presented in Figure 9. The iterative procedure involves taking heat and mass balances for a particular node or shell and then progressing to the next node. When all nodes are completed, the present time for the values of temperature and concentrations for all nodes is switched to the past time for the next time step and the nodal iteration procedure is again repeated for the next time increment. Note that although the explicit solution technique is used, oscillations in temperature and concentrations are precluded by choice of a sufficiently small time increment for calculations. This time increment is estimated by the time constant for heat transfer which is

$$t_c = \frac{1}{2} \left[\frac{\rho C_p (\Delta V) (R \Delta \zeta)}{kA} \right] \qquad (6)$$

where all terms apply to a particular node.

B. Program Listing and Input Data

An example listing for the input data and equations for the PARTIG Program is presented in Figure 10. The input data in this listing is based on a 50μ lithium aluminum hydride particle. The ignition source for this analysis was considered as the hot surrounding gases in a solid propellant rocket chamber at 2500°K since the potential use of these particles as additives in solid rocket propellants may be desirable. Also, for comparisons with the experimental data on powder, the reacting temperatures for powder and the hydrogen flame temperature would be close to 2500°K (from 2200°K up) and would contribute about the same amount toward ignition of a single particle.

For the hydrogen evolution and heat of reaction, the experimental data of Block and Gray[1] as presented in Figures 1 and 2 was used. To simplify calculations, the hydrogen evolved and the heat of reaction were considered to occur as steps at the peak temperatures and the total amounts of hydrogen and heat evolved for each temperature region indicated in these figures was assumed to occur at the temperatures of the peaks.

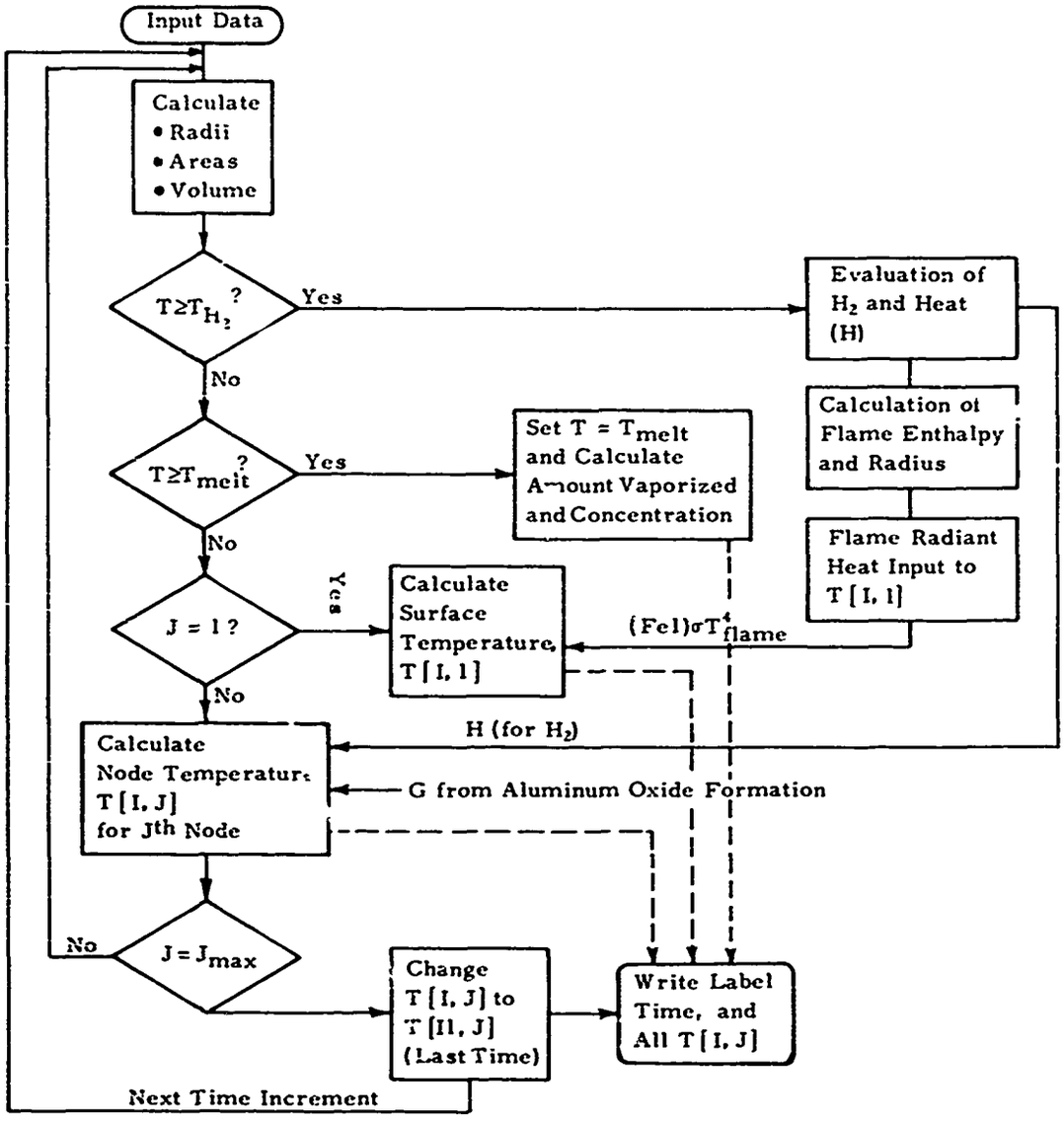

Figure 9. Temperature Analysis Loop for PARTIG Program

```
COMMENT        LI-AL-H4 PARTICLE IGNITIØN ;
          BEGIN
FILE OUT       LINE 4(2,15);
   A M0063     DATELINE ("PARTIG") ;
FORMAT OUT     FMT1(E13.6.X4/11(10(F9.2,X2)/));

FORMAT OUT     SPACE1();

FORMAT OUT     FMT2(E13.6,X4,I3,X4,E13.6,X4,E13.6,X4,E13.6) ;

FORMAT OUT     FMT3(E13.6,X4,E13.6,X4,E13.6);

FORMAT OUT     FMT4(X10,"SHELL TEMPERATURES");

FORMAT OUT     FMT5(X10,"ØXYGEN CØNCENTRATIØN");

FORMAT OUT     FMT6(X10,"ALUMINUM VAPØR CØNCENTRATIØN");

FORMAT OUT     FMT7(X10,"HYDRØGEN PYRØLYSIS");

FORMAT OUT     FMT8(X10,"LIALH4 PARTICLE IGNITIØN, INITIAL VALUES");

FORMAT OUT     FMT9(E13.6,X4/4(6(E13.6,X2)/));

FORMAT OUT     FMT10(X10,"ALUMINUM ØXIDE EQUIVALENT Ø2 CØNCEN.");

INTEGER        J,I,M,I1,J1,B;
INTEGER        Y,Z,D;
REAL           DELE,DELT,R,K1A,RHØ1,CP1A,K2A,RHØ2,CP2A,K3A,RHØ3,CP3A,
               PI,TIME,TIME2,CØND,ALFA,CP,RHØ,TF1,TF2,TF3,TPG1,TPG2,
               TPG3,H,DELH1,G,H2,HØ,HØ1,C1,CPØ,RF,HP,FEPG,FES,FE1,FE2,
               FE3,SIGMA,HPG,HØ25,TPG,QLAS,CPH;
REAL           PØ,LAG,CAC1,CAC2,CBC1,DIFA,DIFB,MELT,LV,CAD,CAØ,ALØ,MAL;
REAL           MØ;
ARRAY          RAD[0:21,0:21], A[0:2 ,0:2] ,DV[0:21] ,T[0:2,0:22] ,HT[0:2];
ARRAY          DELH[0:2,0:22] ,HD[0:2,0:22] ,AL[0:2,0:22] ,ALT[0:2,0:22];
ARRAY          CA[0:2,0:22] ,CB[0:3,0:22] ,TIM[0:2] ,Q[0:2] ,V[0:2];
ARRAY          Ø[0:2,0:22];
LABEL          P1;
LABEL          P2 ;
               FØR J←1 STEP 1 UNTIL 6  DØ
          BEGIN Ø[1,J]←0;
               CB[1,J]←0.0;
               CA[1,J]←0;
               T[1,J]←300;
               TIME←0.0
          END;
               WRITE(LINE,FMT8);
               WRITE(LINE,FMT4);
               WRITE(LINE,FMT1,TIME,FØR J←1 STEP 1 UNTIL 6    DØ T[1,J]);
```

Figure 10. Listing for the PARTIC Program - As Run for $LiAlH_4$ Ignition

```
WRITE(LINE,FMT5);
WRITE(LINE,FMT9,TIME,FØR J←1 STEP 1 UNTIL 6   DØ
 CA[1,J]);
WRITE(LINE,FMT6);
WRITE(LINE,FMT9,TIME,FØR J←1 STEP 1 UNTIL 6   DØ
 CB[1,J]);
WRITE(LINE,SPACE1);
DELE←0.200;
DELT←1.00@-6 ;
R←2.5@-3;
Y←0;
Z←0;
DIFA←0.200;
DIFB←0.150;
PØ←1.0;
LAG←25;
CAC1←0;
CAC2←7.81@-10;
CBC1←1.04@-9;
MELT←991;
MØ←16.0;
Q[I]←0;
CA0←8.2@-7;
V[I]←0;
ALØ←3900;
LV←2360;
MAL←26.97;
D←1;
K1A←9.09@-3;
RHØ1←0.917;
 CP1A←0.200;
K2A←9.09@-3;
RHØ2←0.820;
CP2A←9.200;
SIGMA←1.365@-12;
PI←3.1416;
TPG1←2500;
TPG2←0;
TPG3←0;
TF1←443;
TF2←2320;
TF3←0 ;
CAD←RHØ2@MO/(2.0@MAL);
HØ25←0 ;
CBØ←0.262 ;
FEPG←1.00 ;
FES←0.90 ;
CPH←3.25 ;
HP←1.43@4;
I←2;
I1←I-1;
TPG←TR[1 ;
HPG←1.6@-2 ;
QLAS←0.0;
FØR J←1 STEP 1 UNTIL 6   DØ
```

Figure 10. (Continued)

```
BEGIN
     J1←J-1;
     RAD[J1,1]←R@(1-(J1-1)@DELE);
     RAD[J1,2]←R@(1-J1@DELE);
     A[J1,1]←4@PI@RAD[J1,1]*2 ;
     A[J1,2]←4@PI@RAD[J1,2]*2 ;
     DV[J1]←4/3@(RAD[J1,1]*3-RAD[J1,2]*3)@PI;
     IF J=2 THEN B←2 ELSE B←1 ;
     IF T[I1,J] = 723 THEN
BEGIN
     C@ND←K2A;
     CP←CP2A;
      RH@←RH@2;
END  ELSE
BEGIN
     C@ND←K1A;
     CP←CP1A;
     RH@←RH@1;
END;
     IF T[I1,J]≥TF1 THEN
BEGIN DELH[I,J]←56.9; C1←1.88@ 5
END;
     IF T[I1,J]≥ 483 THEN
BEGIN DELH[I,J] ←115.4; C1 ←8.51@ 4
 END;
     IF T[I1,J] ≥ 548 THEN
BEGIN DELH[I,J]←166.6; C1←4.86@ 4
END;
     IF T[I1,J] ≥ 723 THEN
BEGIN DELH[I,J]←327.6; C1←1.45@ 4
END;
     IF J=1 THEN H←0 ELSE
BEGIN
     H←DV[J]@(DELH[I,J]-DELH[I1,J]);
      H2←C1@H ;
     H@←CP@@(TRG-298) +H@25;
     HD[I,J]←H2@(HP-0.5@H@-CPH@(T[I1,J]-298));
     IF H≠0 THEN
BEGIN  WRITE(LINE,FMT7);
     WRITE(LINE,FMT2,TIME,J1,H2,HD[I,J]);
END;
END;
     IF T[I1,6] > 723 THEN
BEGIN
        TIM [Y]←TIME;
     Y←1;
     IF TIME≥ TIM [0]+LAG@DELT THEN
BEGIN  Z←1.0;
     IF CA[I1,J] ≥ CAC1 THEN
BEGIN  Q[I]←1.0;
     D←2;
     G←2@(Q[I]-Q[I1])@DV[J1]@AL@@M@@(CAD-@[2,J]);
END; IF J=1 THEN CA[I,J]←Z@CA@
     ELSE CA[I,J]← Z@(CA[I1,J]+DIFA@DELT/(DELE@DV[J1]) (A[J1,1]
    @(CA[I1,J1]-CA[I1,J])-A[J1,2]@(CA[I1,J]-CA[I1,J+1]))/R)
```

Figure 10. (Continued)

```
      -(Q[I]-Q[I1])⊗(CAD-Ø[2,J]);
    IF CA[I,J] <0 THEN
BEGIN Ø[2,J]←Ø[1,J] +Z⊗(CA[I1,J]+DIFA⊗DELT/(DELE⊗DV[J1]⊗R)
     ⊗(A[J1,1]⊗(CA[I1,J1]-CA[I1,J])
      -A[J1,2]⊗(CA[I1,J]-CA[I1,J+1])));
    IF Ø[1,J] > CAD THEN CA[I,J]←Ø[1,J]-CAD ELSE
BEGIN CA[I,J]←0;
    Q[I]←0;
    G←2⊗DV[J1]⊗ALØ⊗MØ⊗(Ø[2,J]-Ø[1,J]);
END; Ø[1,J]←Ø[2,J];
END;
END;
END;
    IF T[I1,J] ≥ MELT AND D=1 THEN
BEGIN V[I]←1.0;
    IF ALT[I1,J] ≥ LV⊗DV[J1]⊗RHØ2 THEN AL[I,J]←0 ELSE
BEGIN  IF J=1 THEN AL[I,J]←0 ELSE
    AL[I,J]←CØND/(R⊗DELE)⊗(B⊗A[J1,1]⊗(T[I1,J1]-T[I1,J])
     -A[J1,2]⊗(T[I1,J]-T[I1,J+1]))⊗DELT;
END;
    CB[I,J]←CB[I1,J]-DIFA⊗DELT/(DELE⊗DV[J1])⊗(A[J1,1]
    ⊗(CB[I1,J1]-CB[I1,J])-A[J1,2]⊗(CB[I1,J]-CB[I1,J+1]))/R
     +(V[I]-V[I1])⊗MAL⊗AL[I,J]/(DV[J1]⊗LV);
    ALT[I,J]←ALT[I1,J]+AL[I,J];
END  ELSE AL[I,J]←0;
    ALFA←CØND/(RHØ⊗CP) ;
    IF J=1 THEN
     T[I,J]←T[I1,2]+DELE/(2⊗CØND)⊗(HPG⊗(TPG-T[I1,1])
      +SIGMA⊗(FEPG⊗TPG↑4-FES⊗T[I1,1]↑4+FE1⊗TF2↑4))⊗R
    ELSE
     T[I,J]←T[I1,J]+ALFA⊗DELT/(R⊗DELE⊗DV[J1])⊗(B⊗A[J1,1]⊗
     (T[I1,J1]-T[I1,J])-A[J1,2]⊗(T[I1,J]-T[I1,J+1]))
      +DELT/(RHØ⊗CP⊗DV[J1])⊗(H+G-AL[I,J]);
END;
    TIME2←TIME + DELT ;
    HT[I]←HD[I,1]+HD[I,2]+HD[I,3]+HD[I,4]+HD[I,5]+HD[I,6];
    IF HT[I]-HT[I1]=0 THEN RF←R       ELSE
    RF←R⊗HT[I]/(HT[I]-HT[I1])⊗PØ;
    WRITE (LINE,FMT3,TIME2,HT[I],RF);
    WRITE(LINE,FMT4);
    WRITE(LINE,FMT1,TIME2,FØR J←1 STEP 1 UNTIL 6  DØ T[I,J]);
    WRITE(LINE,FMT5);
    WRITE(LINE,FMT9,TIME2,FØR J←1 STEP 1 UNTIL 6  DØ
     CA[I,J]);
     WRITE(LINE,FMT10);
    WRITE(LINE,FMT9,TIME2,FØR J←1 STEP 1 UNTIL 6  DØ
     Ø[1,J]);
    WRITE(LINE,FMT6);
    WRITE(LINE,FMT9,TIME2,FØR J  1 STEP 1 UNTIL 6  DØ
     CB[I,J]);
    WRITE(LINE,SPACE1)
    FØR M←1 STEP 1  UNTIL 6   DØ
BEGIN T[1,M]←T[2,M];
    HT[1]←HT[2];
```

Figure 10. (Continued)

```
                DELH[1,M]←DELH[2,M];
                TIME←TIME2;
                CA[1,M]←CA[2,M];
                CB[1,M]←CB[2,M];
                ALT[1,M]←ALT[2,M];
                HD[1,M]←HD[2,M];
                Q[1]←Q[2];
                V[1]←V[2];
            END;
                IF TIME  DELT≤10000 THEN GØ TØ P1;
P2:             DATELINE(0) ;
            END.
```

Figure 10. (Continued)

For the program, the input values selected for thermal and physical properties are indicated on the listing (Figure 10) on cards 36 through 78. The effective mass diffusivities, DIFA and DIFB, were estimated from values for molecular diffusivity tabulated in Bird, Stewart and Lightfoot.[4] These values for molecular diffusivity corrected to effective diffusivity for the porous pellet by using effectiveness corrections from Petersen.[6] Also, a temperature correction of $T^{3/2}$ for the average temperature was corrected to effective diffusivity for the porous pellet by using effectiveness corrections from Petersen.[6] Also, a temperature correction of $T^{3/2}$ for the average temperature was applied based on the Chapman-Enskog equation as presented in Bird, Stewart and Lightfoot[4] assuming a perfect gas.

The critical concentrations were not available for a 2500°K environment and some of the other properties were estimated. Thermal and physical constants such as heats of reaction and vaporization, thermal conductivity, and density were based on data from Perry,[7] the CRC Handbook[8] and the JANAF Tables.[9] Since, during the pyrolysis of hydrogen and other steps, it is not clear whether or not the total lithium content is pyrolyzed, the melting temperature for the core, MELT, is based on two-phase data on the melting temperature of Li-Al from Hansen.[10]

The convective heat transfer coefficient HPG was estimated for free convection assuming that the particle was at rest relative to the surrounding environment. According to McAdams,[11] data has been presented which indicates that for small particles (below ~ 1/4 inch in diameter) the Nusselt number approaches a constant value which is close to or actually the transfer value due to gaseous conduction.

IV. DISCUSSION

The results of this investigation are in general agreement with the kinetic mechanism proposed by previous investigators.[1,2] Garner and Haycock investigated the isothermal decomposition of Lithium Tetrahydraluminate and found a reaction sequence corresponding to the formal equation

1. $LiAlH_4 \rightarrow LiAlH_2 + H_2$
2. $LiAlH_2 \rightarrow LiH + Al + \frac{1}{2}H_2$

Block and Gray modified this reaction sequence by including

3. $LiH \rightarrow Li + \frac{1}{2}H_2$.

These workers utilized a slow pyrolysis during which the sample was heated at a rate of temperature rise approximately 10° 1 min. Although the present work has a much higher thermal rise rate, the general reaction sequence appears to be basically similar. The spectrographic studies are characterized by the onset of an atomic lithium emission line at relatively low temperatures. This emission remains at a constant "temperature" for a considerable length of time. There then follows a discrete increase in the intensity of emission in which additional atomic lithium lines are activated indicating an increased reaction temperature. This condition forms a discrete second stage which is then followed by an afterburning of the residual substrate. The sequence supports a reaction mechanism which can be described by the following equations:

Step 1
- 1a. $LiAlH_4 \rightarrow LiAlH_2 + H_2$
- 1b. $LiAlH_4 \rightarrow LiH + AlH_3$
- 1c. $LiH \rightarrow Li + \frac{1}{2}H_2$

Step 2
- 2a. $LiAlH_2 \rightarrow LiH + \frac{1}{2}H_2 + Al$
- 2b. $LiH \rightarrow Li + H_2$

Step 3 $Al + O_2 \rightarrow Al_2O_3$.

The principle difference in this mechanism is that it is necessary to include an additional early step which can produce atomic lithium. This could entail a diffusion of the lithium atom from an internal site

to the surface or a disproportionation to form lithium hydride and aluminum hydride. Alternatively the early intense lithium emission could also be explained as "steady state" equilibrization of reactions 1 and 2 of Block and Gray. However, if this were occurring, then a more gradual buildup to the second stage of the reaction would be anticipated.

Results for the PARTIG Program are shown in Figure 11 in which time and temperatures and concentrations are indicated for each node. Also, the hydrogen evolved and heat of evolution are listed at the appropriate peak temperature in Figure 12. Due to the use of discrete peak temperatures the hydrogen evolution appears as "spikes." An estimate of the flame shape for a more continuous modified Arrhenius hydrogen evolution is indicated by the dashed line on the figure. The Phase I ignition would appear to start at about 0.3 milliseconds.

Theoretical prediction for the temperatures of the surface and at the center of the particle are presented in Figure 12. The results indicate a linear rise in temperature with time with no visible perturbations (at the scale of the figure) of temperature due to heat generated from chemical reactions within the nodes. It is noted that the lag between the temperature of the surface and the center of the particle is almost constant at only 10°K. The lag time and diffusion of oxygen into the surface after hydrogen pyrolysis did not appear to affect the temperature. Also, since the concentration of oxygen in the atmosphere is rather low, the formation of aluminum oxide was limited to an extremely thin layer. Because the oxygen diffused into the particle was consumed rapidly near the surface, no concentration was available for reaction with the metal vapor as the core reached melting temperature. Therefore, the Stage II ignition was assumed to take place as soon as the vaporized metal began to diffuse to the surface. Although the 991°K melting temperature is probably not sufficient for ignition, the 2500°K surrounding environment was considered adequate to almost instantaneously bring the metal vapor to the ignition temperature. Based on this assumption, the Stage II ignition occurs at about 1.6 milliseconds.

The reduced experimental results as presented in Figures 4, 5 and 6 were compared with the analytical predictions (Figure 12 and 13) and the results are presented on Figure 14. The 50μ particle delay times from the program were normalized to the 75μ diameter by use of the D^2 law for comparison purposes. The comparison indicates that the analytically predicted Stage I and Stage II ignition times are in close agreement with the observed experimental data for an O/F ratio of 1.0.

```
        LIALH4 PARTICLE IGNITION, INITIAL VALUES
        SHELL TEMPERATURES
0.000000E+00
  300.00      300.00      300.00      300.00      300.00      300.00
        OXYGEN CONCENTRATION
0.000000E+00
0.000000E+00   0.000000E+00   0.000000E+00   0.000000E+00   0.000000E+00   0.000000E+00

        ALUMINUM VAPOR CONCENTRATION
0.000000E+00
0.000000E+00   0.000000E+00   0.000000E+00   0.000000E+00   0.000000E+00   0.000000E+00


4.000000E-07     0.000000E+00     2.500000E-03
        SHELL TEMPERATURES
4.000000E-07
  302.43      300.00      300.00      300.00      300.00      300.00
        OXYGEN CONCENTRATION
4.000000E-07
0.000000E+00   0.000000E+00   0.000000E+00   0.000000E+00   0.000000E+00   0.000000E+00

        ALUMINUM VAPOR CONCENTRATION
4.000000E-07
0.000000E+00   0.000000E+00   0.000000E+00   0.000000E+00   0.000000E+00   0.000000E+00


8.000000E-07     0.000000E+00     2.500000E-03
        SHELL TEMPERATURES
8.000000E-07
  302.43      301.49      300.00      300.00      300.00      300.00
        OXYGEN CONCENTRATION
8.000000E-07
0.000000E+00   0.000000E+00   0.000000E+00   0.000000E+00   0.000000E+00   0.000000E+00

        ALUMINUM VAPOR CONCENTRATION
8.000000E-07
0.000000E+00   0.000000E+00   0.000000E+00   0.000000E+00   0.000000E+00   0.000000E+00


1.200000E-06     0.000000E+00     2.500000E-03
        SHELL TEMPERATURES
1.200000E-06
  303.92      301.78      300.48      300.00      300.00      300.00
        OXYGEN CONCENTRATION
1.200000E-06
0.000000E+00   0.000000E+00   0.000000E+00   0.000000E+00   0.000000E+00   0.000000E+00

        ALUMINUM VAPOR CONCENTRATION
1.200000E-06
0.000000E+00   0.000000E+00   0.000000E+00   0.000000E+00   0.000000E+00   0.000000E+00


1.600000E-06     0.000000E+00     2.500000E-03
        SHELL TEMPERATURES
1.600000E-06
```

Figure 11. PARTIG Program Printout Results - Example for $LiAlH_4$

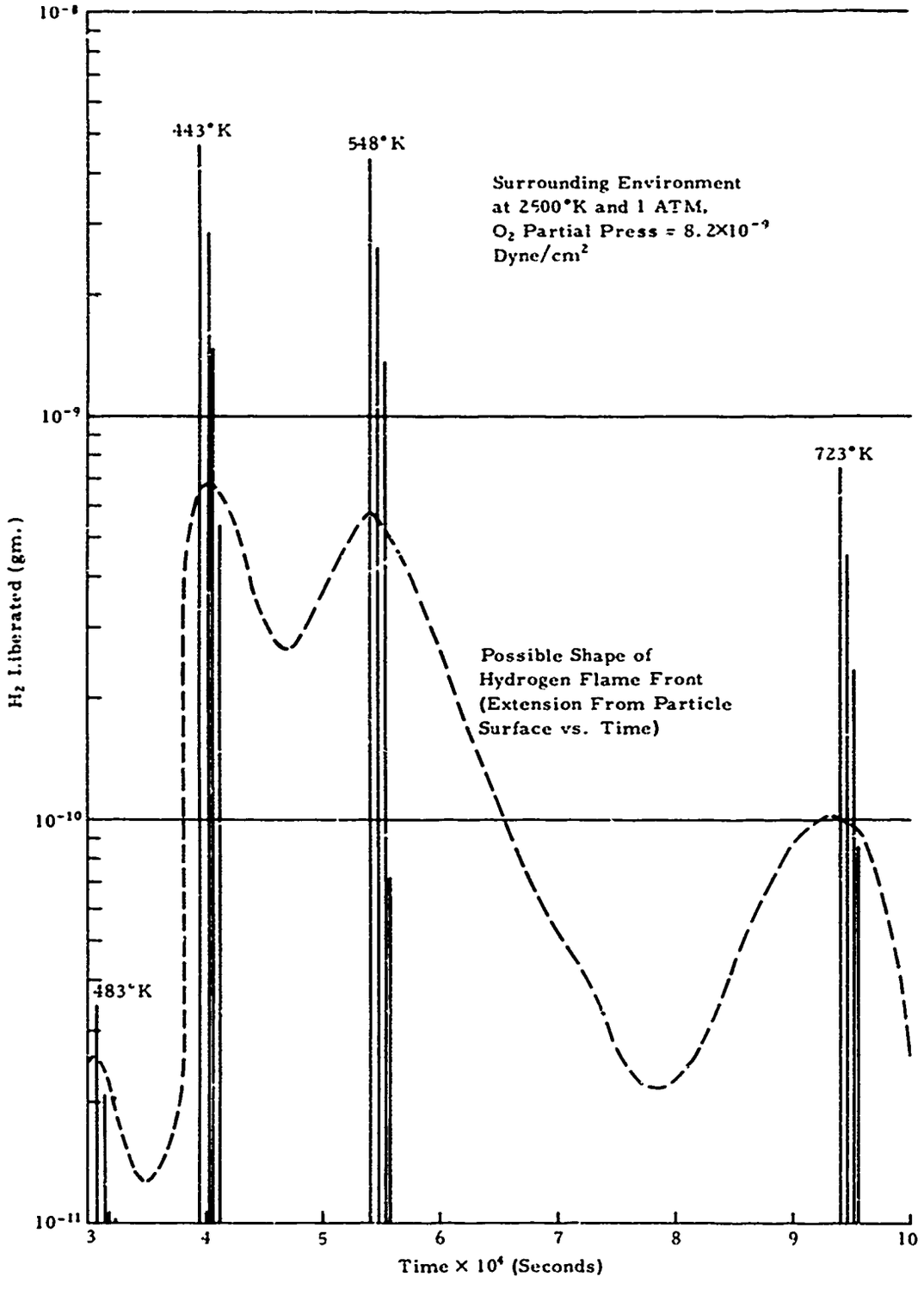

Figure 12. $LiAlH_4$ Hydrogen Pyrolysis Analytical Results

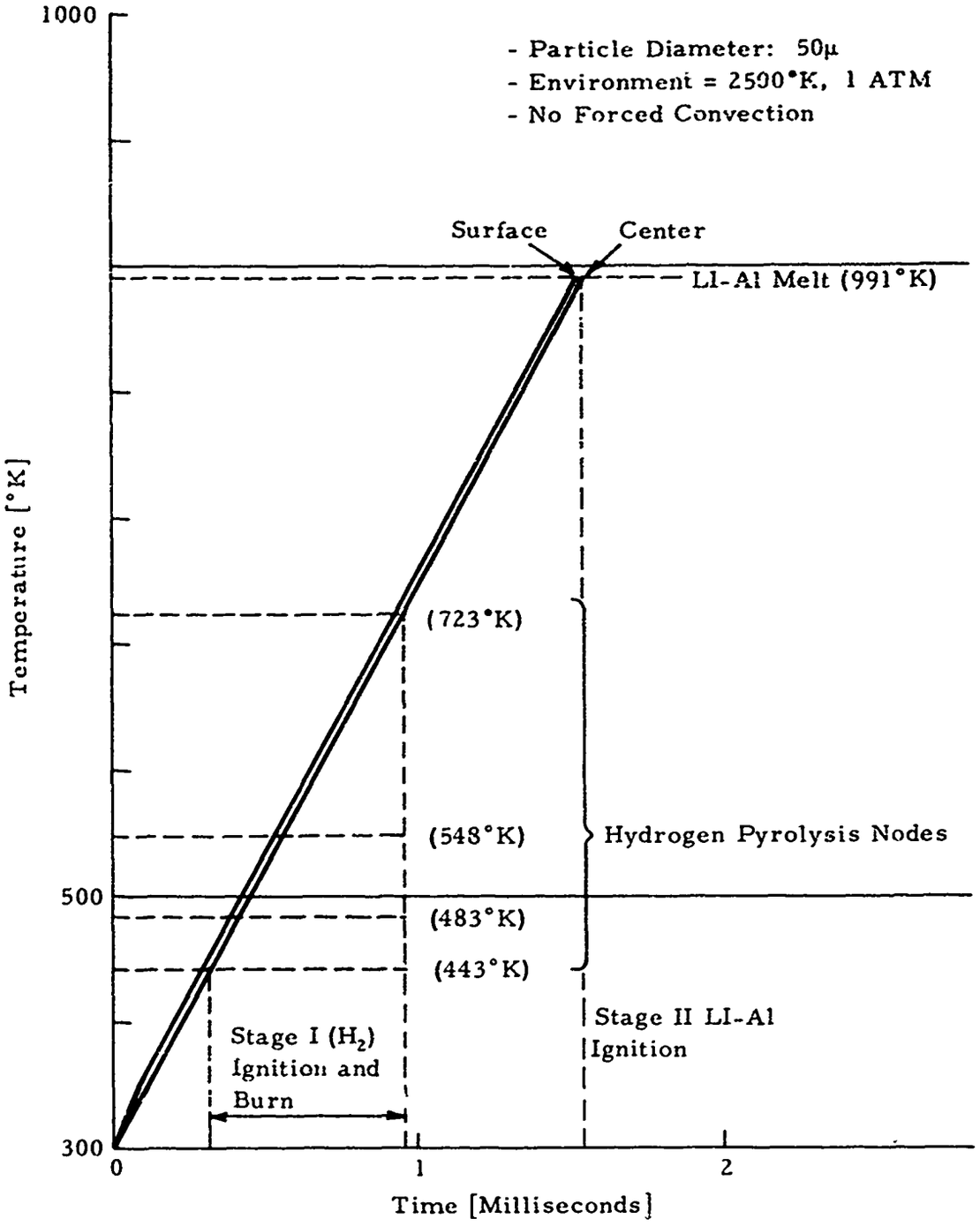

Figure 13. $LiAlH_4$ Particle Temperatures and Ignition Times from PARTIG Program

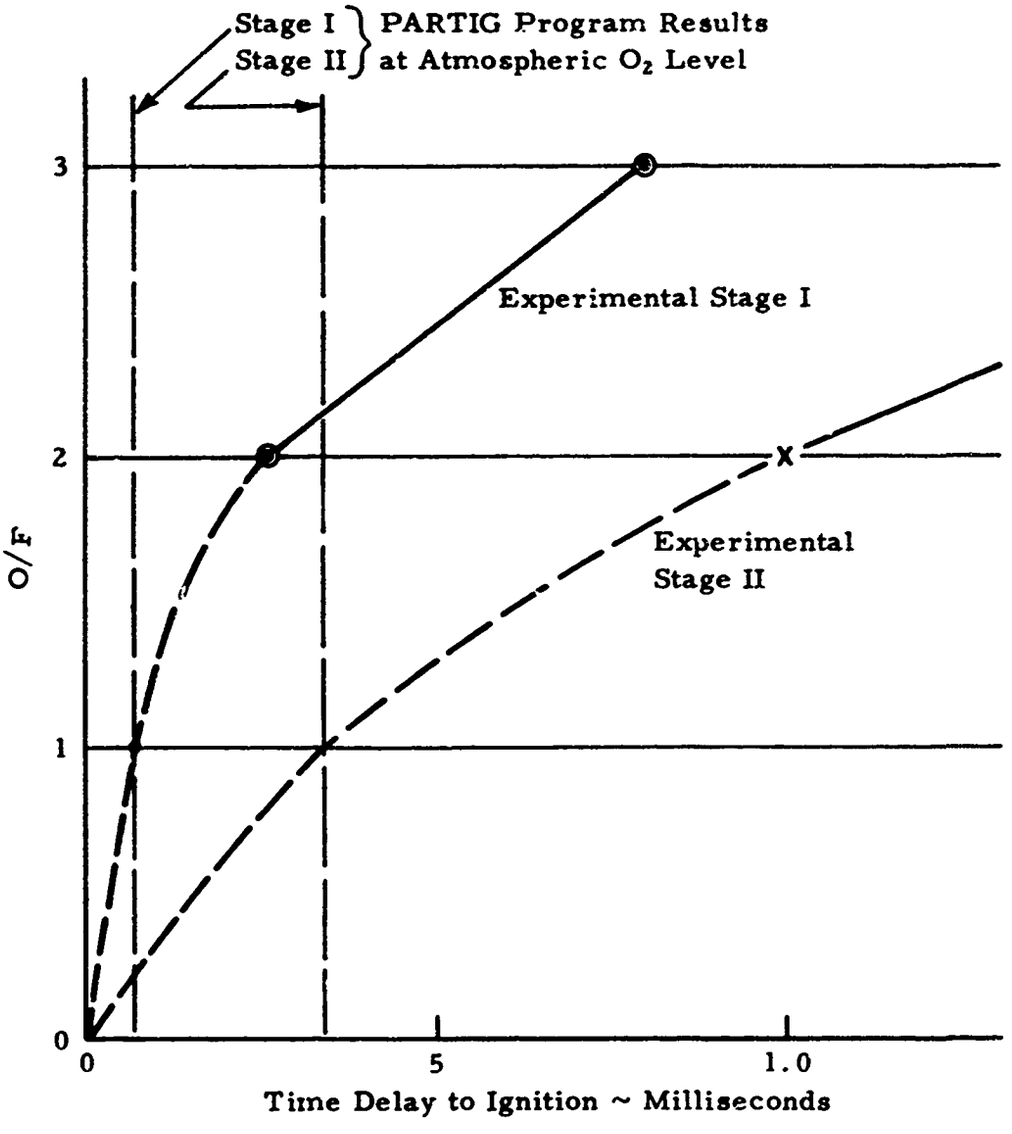

Figure 14. Comparison of Analytical and Experimental Results

Although this comparison appears to confirm the delays estimated by the PARTIG Program, the analytical and experimental conditions differed considerably for oxidizer. Because of these differences, additional analytical solutions with the PARTIG Program will be needed in order to completely verify the accuracy of the program for predicting ignition times.

V. CONCLUSIONS

A number of conclusions can be formulated even with limited data presently available.

1. This simple combustion model used to describe the combustion of molten metal spheres requires modification to account for a multistage reaction sequence in which the "cool flame" pyrolysis is followed by a "hot flame" combustion zone.

2. The time lag required for the ignition of the particle is strongly dependent on the particle size and surface areas and varies as a function of the O/F mixture ratio.

3. Prediction of ignition delay times for multistaged ignition in porous light metal hydride particles can be described using a nodal shell balance analysis.

4. The analytical and experimental results are in reasonable agreement and tend to confirm the assumed theoretical model for multistage pyrolysis and combustion of light metal hydride particles.

From an engineering point of view, the results of this program indicate that the stepwise pyrolysis of a metal hydride must be considered in order to insure efficient combustion. For example, the optimization of a propellant surface regression rate is dependent, in part, on the time required for the pyrolysis of the hydride component. The reported information can be used in two ways: (1) to determine the maximum particle size necessary for the complete combustion of the slow-burning fuel component, and (2) to control ignition spiking. The necessary particle size can be estimated for these propellants from an examination of Figure 4. Ignition spiking can be reduced by placing a hydride layer on the propellant surface and using the built-in reaction stages to control pressure rise rates at a minimal impulse loss. An estimate of the time delay can be developed through reference to Figures 5 and 6.

REFERENCES

1. Block, Jacob and Gray, A. P., J. Inorg. Chem., 304-305, 4, (1965).

2. Garner, W. E., and Haycock, E. W., Proc. Roy. Soc. (London), 335, A111 (1952).

3. Brzustowski, Thomas A., Vapor-Phase Diffusion Flames in the Combustion of Magnesium and Aluminum. Ph.D. Dissertation at Princeton University; 63-8133, University Microfilms, Inc., Ann Arbor, Michigan (1963).

4. Bird, R. B., Stewart, W. E., and Lightfoot, E. N., Transport Phenomena. John Wiley and Sons, New York (1960).

5. Kuehl, D. K., and Zwillenberg, M. L., "Predictions of Burning Times of Metal Particles." AIAA Paper No. 68-494, presented at the ICRPG/AIAA Third Solid Propulsion Conference, Atlantic City, N. J. (June 1968).

6. Petersen, E. E., Chemical Reaction Analysis. Prentice-Hall, Inc., New Jersey (1965).

7. Perry, J. H., Editor, Chemical Engineer's Handbook. McGraw-Hill Book Company, Inc., New York (1950).

8. C. R. C. Handbook of Chemistry and Physics. 46th Edition, The Chemical Rubber Company (1966).

9. JANAF Thermochemical Tables.

10. Hansen, Max, Constitution of Binary Alloys. McGraw-Hill Book Company, Inc. (1958).

11. McAdams, W. H., Heat Transmission, McGraw-Hill Book Company, Inc. (1954).

APPENDIX A. NOMENCLATURE

A. Text

A	Area
C	Molar concentration
C'	Molar concentration, present time interval
C_p	Specific heat at constant pressure
D_e	Effective mass diffusivity
k	Thermal conductivity
k_1	Constant for reaction kinetics
m	Mass
n	Order of reaction
O/F	Oxygen/fuel ratio
q	Heating rate from reactions
R	Radius of particle
$R_1, R_2 \ldots$	Radii of nodal surfaces
t	Time
t_c	Time constant for conductive heat transfer
T	Temperature
T'	Temperature, present time interval
ΔV	Incremental volume of node
x	Distance between node centers
ρ	Density
$\Delta\zeta$	Ratio of nodal shell rings to total radius, $\Delta R/R$
μ	Micron

Subscripts:

1, 2 . . .	Nodes
melt.	Melting

B. PARTIG Program Nomenclature

A[J1, 1]	Surface area into shell J - 1
A[J1, 2]	Surface area from shell J - 1
ALFA	Thermal diffusivity
AL[I, J]	Incremental amount of metal vaporized
ALO	Heat of formation of aluminum oxide
ALT[I, J]	Total amount of metal vaporized
B	Integer, B = 2 for J = 1, B = 1 otherwise

C1	Ratio (H_2/AlH_3)
CA[I, J]	Molecular concentration of species A
CAC1	Critical concentration of A for first ignition
CAC2	Critical concentration of A for second ignition
CAD	Concentration capacity of reaction with A
CB[I, J]	Molecular concentration of species B
CBC1	Critical concentration of B for first ignition
COND	Thermal conductivity
CP1A, CP1B, CP1C	Specific heat constants for material #1 with $CP = CP1A + CP1B(T) + CP1C(T)^2$
CP2A, CP2B, CP2C	Specific heat constants for material #2 with $CP = CP2A + CP2B(T) + CP2C(T)^2$
CP3A, CP3B, CP3C	Specific heat constants for material #3 with $CP = CP3A + CP3B(T) + CP3C(T)^3$
CPH	Specific heat of hydrogen
CPO	Specific heat of oxygen
D	Integer, D = 2 for Al_2O_3, D = 1 otherwise
DELE	Incremental distance between shells
DELH1	Enthalpy change for evolution of H_2, cal/gm
DELH[I, J]	Enthalpy change for J^{th} node, cal/gm
DELT	Incremental step change in time
DIFA	Mass diffusivity of species A
DIFB	Mass diffusivity of species B
DV[J1]	Incremental volume for J1 shell
FE1	Combined emissivity factor for H_2 flame front
FE2	Combined emissivity factor for Al flame front
FEPG	Combined emissivity factor for propellant gases
FES	Combined emissivity factor for particle surface
G	Enthalpy change for oxide formation
H	Enthalpy change for H_2 pyrolysis
H2	Amount of hydrogen liberated
HO	Enthalpy of O_2 for H_2 pyrolysis
HO25	Base value of O_2 enthalpy at 25°C
HD[I, J]	Enthalpy of products for H_2-O_2 reaction

HP	H_2 pyrolysis reaction energy
HPG	Heat transfer coefficient for propellant gases to particle surface
HT[I]	Total enthalpy for H_2-O_2 reaction
I	Integer for present time increment
II	Integer (I - 1) for previous time increment
J	Integer for J^{th} particle shell
J1	Integer for J - 1 particle shell
K1A, K1B, K1C	Thermal conductivity constants for material #1 COND = K1A + K1B(T) + K1C$(T)^2$
K2A, K2B, K2C	Thermal conductivity constants for material #2
K3A, K3B, K3C	Thermal conductivity constants for material #3
LAG	Number of lag time increments before oxygen back-diffusion
LV	Latent heat of vaporization of metal
M	Integer for time conversion from I to II
MAL	Molecular weight of aluminum
MELT	Melting temperature of metal
MO	Molecular weight of oxygen
P1, P2	Labels
PI	pi (3.1416)
PO	Partial pressure ratio of oxygen to 1 atmosphere
Q[I]	Switching integer (1 or 0)
QLAS	Laser heat input
R	Radius of particle
RAD[J1, 1]	Radius into J1 shell
RAD[J1, 2]	Radius inwards from J1 shell
RF	Flame front radius for H_2-O_2 reaction
RHO	Density
RHO1	Density of material #1
RHO2	Density of material #2
RHO3	Density of material #3

SIGMA	Stefan-Boltzmann constant
T[I, J]	Temperature of the J^{th} shell at the present time
T[I1, J]	Temperature of the J^{th} shell at the previous time
TIM[I]	Time at end of hydrogen pyrolysis
TIME	Present time
TIME2	Next time (TIME + DELT)
TF1	Temperature of reaction for H_2 pyrolysis
TF2	Temperature of reaction for oxide formation
TF3	Reaction temperature for metal ignition
TPG	Environment gas temperature
TPG1, TPG2, TPG3	Constants for propellant gases temperature $TPG = TPG1 + TPG2(TIME) + TPG3(TIME)^2$
V[I]	Switching integer (1 or 0)
Y	Integer
Z	Switching integer (1 or 0)

Note: Any consistent system of units may be used for the program. c.g.s. units were used by the authors.

UNCLASSIFIED

Security Classification

DOCUMENT CONTROL DATA - R & D

Security classification of title, body of abstract and indexing annotation must be entered when the overall report is classified

1. ORIGINATING ACTIVITY (Corporate author)
University of Denver
Colorado Seminary
Denver, Colorado 80210

2a. REPORT SECURITY CLASSIFICATION
Unclassified

2b. GROUP

3. REPORT TITLE
Pyrolysis and Combustion of Lithium Aluminum Hydride

4. DESCRIPTIVE NOTES (Type of report and inclusive dates)
Scientific Final

5. AUTHOR(S) (First name, middle initial, last name)
William H. McLain
Franklin I. Honea

6. REPORT DATE
May 1969

7a. TOTAL NO. OF PAGES
39

7b. NO. OF REFS
11

8a. CONTRACT OR GRANT NO.
AF AFOSR-1079-66

b. PROJECT NO. 9711-01

c. 6144501F

d. 681308

9a. ORIGINATOR'S REPORT NUMBER(S)
DRI #2504

9b. OTHER REPORT NO(S) (Any other numbers that may be assigned this report)
AFOSR 69-2052TR

10. DISTRIBUTION STATEMENT
This document has been approved for public release and sale; its distribution is unlimited

11. SUPPLEMENTARY NOTES
TECH, OTHER

12. SPONSORING MILITARY ACTIVITY
AF Office of Scientific Research (SREP)
1400 Wilson Boulevard
Arlington, Virginia 22209

13. ABSTRACT

The slow pyrolysis of lithium aluminum hydride proceeds by a successive dehydrogenation of the fuel in three stages over a temperature range between 210° and 460°C. The combustion of lithium aluminum hydride follows a simular multistage process in which the pyrolytic dehydrogenation is followed by an afterburning of the metal substrate. Experimental studies were performed to determine the delay times between successive stages for solid mixtures of lithium aluminum hydride with selected oxidizers. Time resolved spectrographic techniques were used to determine the duration of these stages. Studies were performed using Li_2O_2 and NH_4NO_3 oxidizers over a particle size range between 75-300 microns and O/F mixture ratios of between 0.5 and 3.0. Ignition delay times for the initial reaction were found to vary between 5 and 40 milliseconds for the first stage and 10 to 120 milliseconds for the second stages. An analytical model was developed to describe the observed multistage combustion process. The model and resulting PARTIG computer program utilize the nodal approach with stepwise solution of the equations for heat and mass transfer. The analytically predicted ignition delay times for a 50μ particle agreed favorably with the experimentally obtained times.

DD FORM 1 NOV 65 1473 (PAGE 1)

S/N 0101-807-6801

UNCLASSIFIED

Security Classification

UNCLASSIFIED

Security Classification

14 KEY WORDS	LINK A		LINK B		LINK C	
	ROLE	WT	ROLE	WT	ROLE	WT
Light Metal Hydride						
Pyrolysis						
Lithium Aluminum Hydride						
Ignition						
Particle Combustion						

DD FORM 1 NOV 65 1473 (BACK)

(PAGE 2)

UNCLASSIFIED

Security Classification